

Charge Transfer with a Spin. I: A Generalized CASSCF Framework for Investigating Charge Transfer in the Presence of Spin–Orbit Coupling

Alok Kumar,^{†,‡} Zhen Tao,[¶] Joseph E. Subotnik,[‡] and Tian Qiu^{*,‡}

[†]*Department of Chemistry, University of Pennsylvania, Philadelphia, Pennsylvania, 19104, USA*

[‡]*Department of Chemistry, Princeton University, Princeton, New Jersey, 08540, USA*

[¶]*Department of Chemistry, University of Rhode Island, Kingston, Rhode Island, 02881, USA*

E-mail: tianq@princeton.edu

Abstract

We present a generalized extension of the recently developed electron/hole-transfer Dynamically-weighted State-Averaged Constrained CASSCF (eDSC/hDSC) method to model charge transfer in the presence of spin-orbit coupling (SOC) for systems containing an odd number of electrons. Our approach incorporates complex-valued spinor orbitals and incorporates four electronic configurations in describing ground-excited state curve crossings between Kramers-restricted doublet states. The method achieves smooth potential energy surfaces and rapid self-consistent field (SCF) convergence across a wide range of spin-orbit coupling strengths, providing an efficient framework

for investigating charge transfer processes in the presence of nontrivial spin degrees of freedom.

1 Introduction

Charge transfer (CT) processes are ubiquitous in nature, playing key roles in photosynthesis^{1,2} and cellular energy conversion processes;^{3–5} CT processes are also at the heart of many modern device applications involving organic electronics^{6–8} and light emitting diodes.^{9–13} Unluckily for the experimentalist (but luckily for the theorist), CT is a very complicated process, the modeling of which is a full time job. On the one hand, it is well known that, in order to maintain energy conservation during a charge transfer process, the electronic and nuclear degrees of freedom must exchange energy; in other words, nuclear dynamics and rearrangement cannot be avoided.^{14–20} On the other hand, by definition, charge transfer processes inevitably involve multiple electronic states and therefore demand an accurate description of static electron-electron correlation—a challenging task, especially for thermal electron transfer, where we must balance the energies of ground and excited states.^{21,22} While a great deal of progress has been made in modeling *ab initio* CT processes, and surface hopping techniques are now routine as far as simulating the nonadiabatic dynamics (the first problem),^{23–26} performing efficient, multireference electronic structure calculations that are just accurate enough remains difficult (the second problem) and is almost always the computational bottleneck preventing large scale simulation.^{27–30}

A few words are now appropriate about how one usually picks out an electronic structure package for running nonadiabatic dynamics to simulate charge transfer. If one seeks to go beyond semi-empirical calculations,³¹ for large scale simulations, one would like to simply model excited states as orbital energies. This approach has been followed for years by Prezhdo and co-workers with some success in the solid state, but it is worth noting that for molecules, orbital energies experience trivial crossings routinely and virtual orbital energies

can be very sensitive to basis set.^{32–34} For two state dynamics, simulating nonadiabatic processes on the ground DFT and excited state TD-DFT states is common nowadays,^{25,35,36} but the downside of such an approach is that when the two surfaces come together, one fails to recover the correct topology of a conical intersection.^{37–39} Interestingly, to our knowledge, very few (if any) nonadiabatic simulations have been run with constrained DFT,^{40–42} which would provide another approach for balancing ground and excited states if merged with configuration interaction (but which might fail for large couplings⁴³). For the most part, as far as simulating nonadiabatic dynamics is concerned today, the most common approach nowadays is to run complete active space self-consistent field (CASSCF) simulations, where one optimizes both the orbital basis and the wavefunction coefficients in that basis at the same time.^{44,45} When properly state-averaged, CASSCF can correctly balance ground and excited states, and thus CASSCF would appear to be the most natural electronic structure approach for running nonadiabatic simulations.

At this point, there are two crucial features of modern CASSCF implementations that must be highlighted. The first point of interest is that, CASSCF very often produces discontinuous potential energy surfaces.⁴⁶ This problem arises because CASSCF can very often find multiple solutions – especially for larger active space (but often even for smaller active spaces). Obviously, running dynamics requires smooth potential energy surfaces (at least smooth far away from conical intersections). To that end, our research group has recently developed a constrained CASSCF algorithm, whereby we mandate that the active space be as small as possible and we further insist that that active space be partitioned appropriately across a donor and acceptor – which is appropriate for electron and hole transfer and strongly limits the number of possible solutions. Thus far, at the cost of a more complicated optimization, we have found global potential energy surfaces that are remarkably smooth.

The second point of interest that must be emphasized is that, to date, most CASSCF implementations have been based on real-valued orbitals.⁴⁷ CASSCF calculations have been implemented and performed in order to accommodate SOC.^{48–53} However, with the exception

of a few papers by Li *et al.*^{54–56} these calculations use real-valued molecular orbitals and complex-valued configuration interaction amplitudes.⁵⁷ This state of affairs is not surprising; if we wish to include spin-orbit coupling within a CASSCF formalism by including complex orbitals, one would need not only to change a great deal of code, but convergence must also be difficult given the need for state averaging and the small size of the SOC. In general, one still usually prefers to solve a CASSCF Hamiltonian without fine structure and then add in SOC perturbatively at the end.⁵⁸ Of course, while helpful, this method cannot be easily applied to nonadiabatic dynamics.

In this paper, our interest is in exploring charge transfer processes between open-shell (radical) species where spin is involved, a scenario where both of CASSCF’s problems listed above appear prominently. In particular, for a system with odd number of electrons with reasonably well defined donor/acceptor fragments, we will present an electronic structure method for modeling a CT curve crossing between a pair of degenerate Kramers doublets,^{59,60} as shown in Fig. 1. As one might imagine, our approach will be to extend the eDSC/hDSC formalism described in Ref.^{46,61} to the case of electronic states with spin. The end result is a fast, balanced and efficient framework for future investigation of coupled nuclear-electronic-spin dynamics during charge transfer.

Before concluding this introduction, we mention that, although we will not study dynamics here, the question of how nuclei, electrons and spin all couple together during the course of a charge transfer event is an important area of current research.^{11,20} For instance, whereas most models of electron transfer are tied to Marcus theory⁶² in some fashion or another, there is a growing consensus that Marcus theory is incomplete when it comes to spin-coupled electron transfer. For instance, there is growing consensus that one must go beyond Marcus theory to model spin-dependent electron transfer, as is observed through the so-called chiral induced spin selectivity (CISS) effect.⁶³ At bottom, one of the problems with Marcus theory is that, just like closed shell Born-Oppenheimer theory, Marcus theory does not take into account electronic momentum and conserves the nuclear (rather than total)

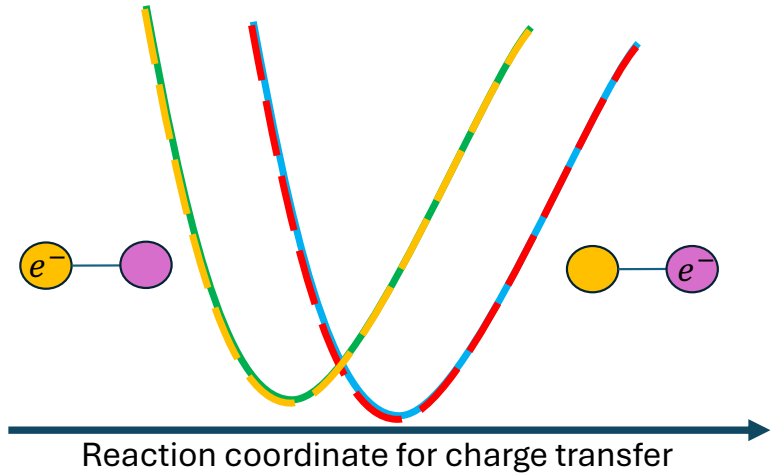


Figure 1: Schematic illustration of crossing between potential energy surfaces (PESs) associated with charge-transfer doublet states in a molecule containing an odd number of electrons. The two diabatic surfaces, correspond to the electron localization of transferring electron on the left or right fragment. The doubly-degenerate nature of each diabat is indicated by colored dashed lines {yellow,green} and {blue, red}.

momentum.^{64–68} To go beyond Marcus theory, and account for both energy conservation *and* momentum conservation will require new dynamical techniques that coupled together nuclear, electronic and spin degrees of freedom – in addition to new electronic structure techniques. Nevertheless, one must crawl before one walks, and we believe that the electronic structure algorithm presented below will help us in our journey. See also Sec. 2.1 below.

With this motivation in mind, an outline of this article is as follows. In Sec. 2, we briefly review the eDSC/hDSC theoretical framework and formulate the Lagrangian with constraints on the active space. In Sec. 2.2, we define the complex-valued spinor basis in which the Fock and density matrix has different spin blocks; in Sec. 2.3 we present the orbital rotation gradients for GHF energy of single Slater determinant; in Sec 2.4, we outline the two step orbital optimization algorithm. The numerical results are presented in Sec. 3. Finally, in Sec. 4, we conclude our work and discuss possibilities for future studies of non-adiabatic process and spin chemistry of charge transfer in odd-number electron systems. As far as notation is concerned, the Greek alphabet will represent the atomic orbitals (AO) and Roman alphabet will represent the molecular orbitals (MO).

2 Method

2.1 Review of eDSC/hDSC

Our treatment of charge transfer in the presence of an unpaired spin is formulated within a Kramers-restricted open-shell framework. By enforcing time-reversal symmetry between paired complex molecular orbitals, the construction becomes directly analogous to restricted open-shell Hartree–Fock (ROHF) and corresponds to the “paired GHF” classification in the Stuber–Paldus scheme.^{69,70} The electronic configurations are thus expressed in terms of complex spinors and their time-reversal partners (see Sec. 2.2), with the resulting wavefunctions naturally occurring in conjugate time-reversal pairs:

$$|\Psi\rangle = |1\bar{1}, 2\bar{2}, \dots, N\bar{N}, N+1\rangle, \quad |\bar{\Psi}\rangle = |\bar{1}1, \bar{2}2, \dots, \bar{N}\bar{N}, \bar{N}+1\rangle \quad (1)$$

where the orbital pairs, like 1 and $\bar{1}$, are time-reversal partners. Following the eDSC/hDSC framework of Qiu and Subotnik,^{46,61} the target function to be minimized is the weighted sum of the energies of these configurations and their time-reversal pairs. The excited configurations are generated through an excitation of an electron (for eDSC) or hole (for hDSC). Because Kramers pairs are degenerate in the absence of time-reversal symmetry breaking (e.g., no external field), it suffices to optimize over a single pair of configurations per state. The total energy is thus given by:

$$E_{\text{tot}} = w_1 E_1 + w_2 E_2 \quad (2)$$

For eDSC, the two configurations are

$$|\Psi_1\rangle = |1\bar{1}, 2\bar{2}, \dots, N\bar{N}, N+1\rangle \quad (3)$$

$$|\Psi_2\rangle = |1\bar{1}, 2\bar{2}, \dots, N\bar{N}, N+2\rangle \quad (4)$$

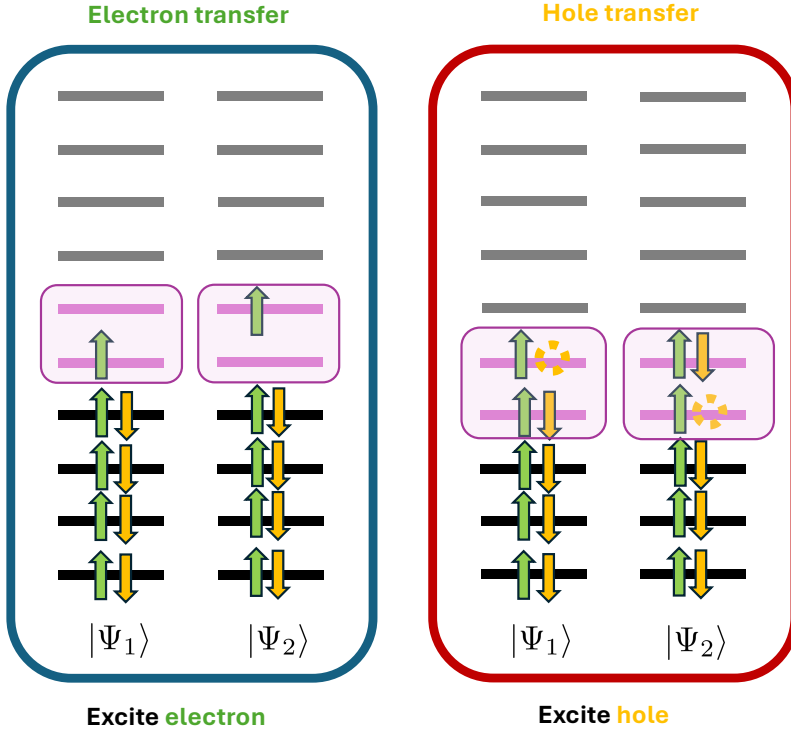


Figure 2: Schematic representation of the active spaces (highlighted in magenta boxes) used to model electron transfer (left) and hole transfer (right) in an open-shell molecular system containing an odd number of electrons. For electron transfer, the active orbitals involve excitation of the unpaired electron, represented by a minimal CASSCF(1,2) active space. The hole-transfer case involves excitation from a doubly occupied orbital, corresponding to a CASSCF(3,2) active space with three electrons distributed over two orbitals.

and for hDSC, the two configurations are

$$|\Psi_1\rangle = |1\bar{1}, 2\bar{2}, \dots, N\bar{N}, N+1\rangle \quad (5)$$

$$|\Psi_2\rangle = |1\bar{1}, 2\bar{2}, \dots, N, N+1, \overline{N+1}\rangle \quad (6)$$

Here, w_1 and w_2 are dynamical weights that depend on a “temperature” parameter T and the energy difference $\Delta E = E_2 - E_1$, where we assume $E_2 > E_1$. As detailed in the original

papers,^{46,61} the weights are proposed to be as follows:

$$w_1(\Delta E) = 1 - \frac{1 - e^{-\Delta E/T}}{2\Delta E/T} \quad (7)$$

$$w_2(\Delta E) = \frac{1 - e^{-\Delta E/T}}{2\Delta E/T} \quad (8)$$

The differential of Eq. 2 is

$$dE_{\text{tot}} = w'_1 dE_1 + w'_2 dE_2 \quad (9)$$

where

$$w'_1 = \left(1 - \frac{1}{2}e^{-\Delta E/T}\right) \quad (10)$$

$$w'_2 = \frac{1}{2}e^{-\Delta E/T} \quad (11)$$

To ensure that the two states correspond to physically meaningful intramolecular charge-transfer configurations rather than spurious local excitations within individual fragments, a constraint is imposed such that the vector space spanned by active orbitals (i.e., orbitals $N + 1$ and $N + 2$ for eDSC and orbitals N and $N + 1$ for hDSC) projects equally onto the vector space spanned by orbitals from the donor (or left, \mathbf{P}_L) and acceptor (or right, \mathbf{P}_R) molecular fragments, i.e.,

$$\text{Tr}(\mathbf{P}_L \mathbf{P}_{\text{active}} - \mathbf{P}_R \mathbf{P}_{\text{active}}) = 0. \quad (12)$$

Using a Lagrangian multiplier, one can write the Lagrangian formally as

$$\mathcal{L} = w_1 E_1 + w_2 E_2 - \lambda \text{Tr}(\mathbf{P}_L \mathbf{P}_{\text{active}} - \mathbf{P}_R \mathbf{P}_{\text{active}}) \quad (13)$$

2.2 Spinor Basis: Complex Molecular Orbitals in Generalized Hartree-Fock

The presence of spin-orbit coupling term in the electronic Hamiltonian mixes the spin components and spatial degrees of freedom. To properly describe such systems, the formulation requires two-component complex-valued spinors which encode both spin and orbital character. We adopt the Generalized Hartree–Fock (GHF) framework,⁷¹ which allows for complex orbital coefficients and arbitrary mixing of α and β spin components. A GHF spin orbital (spinor) can be expanded in terms of real-space atomic orbitals $\phi_\mu(\mathbf{r})$ as

$$\chi_i(\mathbf{r}, \omega) = \psi_i^\alpha(\mathbf{r}) \alpha(\omega) + \psi_i^\beta(\mathbf{r}) \beta(\omega), \quad (14)$$

where

$$\psi_i^\sigma(\mathbf{r}) = \sum_{\mu=1}^K c_{\mu i}^\sigma \phi_\mu(\mathbf{r}), \quad \sigma \in \{\alpha, \beta\} \quad (15)$$

and ω is the spin coordinate and $\alpha(\omega)$ and $\beta(\omega)$ are the orthonormal spin functions corresponding to spin-up and spin-down components, respectively. By arranging the molecular orbital (MO) coefficients in column form, the atomic orbital (AO) basis can be organized into a natural spin-block structure, with distinct $\alpha\alpha$, $\alpha\beta$, $\beta\alpha$, and $\beta\beta$ components. In the ordered AO basis, the density matrix and Fock matrix have a four block structure

$$\mathbf{P} = \begin{pmatrix} \mathbf{P}^{\alpha\alpha} & \mathbf{P}^{\alpha\beta} \\ \mathbf{P}^{\beta\alpha} & \mathbf{P}^{\beta\beta} \end{pmatrix}, \quad \mathbf{F} = \begin{pmatrix} \mathbf{F}^{\alpha\alpha} & \mathbf{F}^{\alpha\beta} \\ \mathbf{F}^{\beta\alpha} & \mathbf{F}^{\beta\beta} \end{pmatrix} \quad (16)$$

The energies of each configuration, E_1 and E_2 depend on the density matrices for ground and excited state, respectively,

$$\mathbf{P}_g = \mathbf{C} \mathbf{K}_g \mathbf{C}^\dagger \quad (17a)$$

$$\mathbf{P}_e = \mathbf{C} \mathbf{K}_e \mathbf{C}^\dagger \quad (17b)$$

which are in turn expressed in term of occupation matrices $\{\mathbf{K}_g, \mathbf{K}_e\}$ as visualized in Fig. 3; here \mathbf{C} is the complex molecular orbital coefficient matrix. The occupation matrix is a diagonal matrix with spin blocks:

$$\mathbf{K}_g = \mathbf{K}_0 + \bar{\mathbf{K}}_0 + \mathbf{K}_1 \quad (18)$$

$$\mathbf{K}_e = \mathbf{K}_0 + \bar{\mathbf{K}}_0 + \mathbf{K}_2 \quad (19)$$

where \mathbf{K}_0 and $\bar{\mathbf{K}}_0$ are the spinor pairs of the Kramers-restricted core orbitals. \mathbf{K}_1 and \mathbf{K}_2 represent the occupancy of the two active space orbitals.

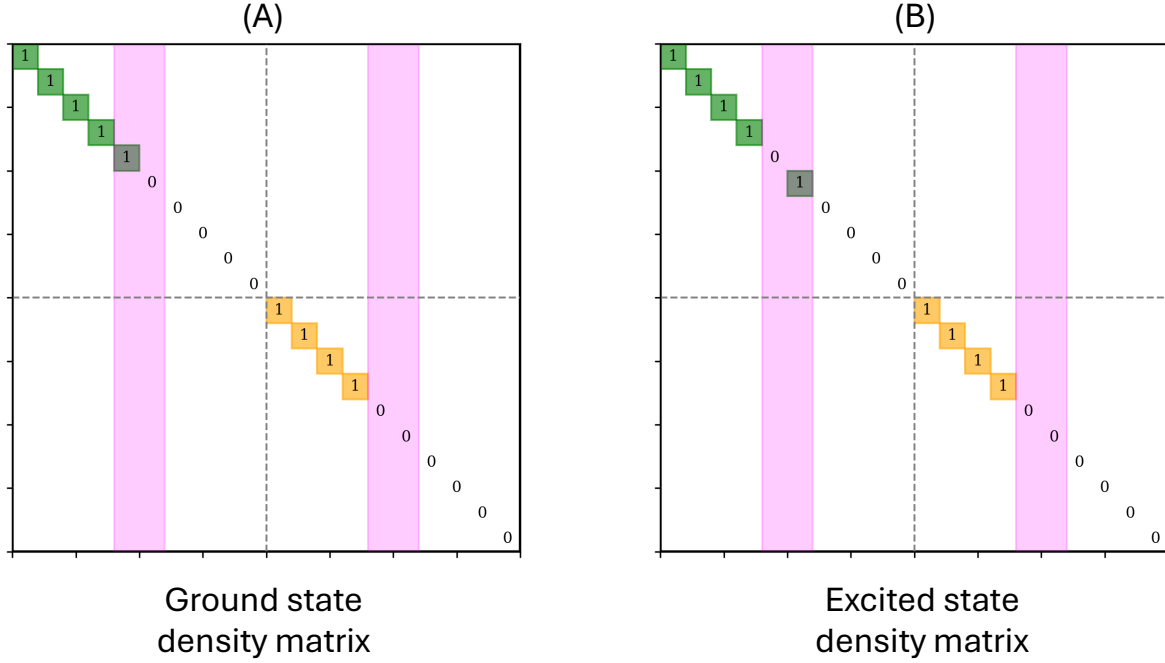


Figure 3: Molecular orbital (MO) density matrices for the (A) ground (\mathbf{K}_g) and (B) excited electronic (\mathbf{K}_e) states. The diagonal elements indicate the occupancies of individual MOs, with pairs of degenerate (Kramers-restricted) orbitals forming two corresponding diagonal sub-blocks (green (1) and yellow ($\bar{1}$)). The magenta columns highlight the active-space orbitals involved in the electronic excitation in the spin-up space. Columns to the left (right) of the active space correspond to core (virtual) orbitals in each half of the matrix.

The single determinant energy of each configuration state can then be expressed as

$$E[\mathbf{P}] = \frac{1}{2} \text{Tr} [(\mathbf{h}_0 + \mathbf{h}_{SO} + \mathbf{F}) \mathbf{P}] \quad (20)$$

where \mathbf{h}_0 is the one electron Hamiltonian and \mathbf{h}_{SO} is the spin-orbit coupling term. The SOC term in Breit–Pauli Hamiltonian contains a one electron part (term arising from the interaction of moving electrons with nuclei) and a two-electron part (made of spin-same-orbit and spin-other orbit contribution).⁷² The one-electron part, being local in nature, is computationally inexpensive to calculate. That being said, it is known that including the two-electron term can decrease the overall magnitude of SOC.⁷³ As such, there are various schemes based on effective one-electron SOC term which account for the contribution from the two-electron part using a mean-field operator,^{74–76} an effective nuclear charge⁷⁷ or other screening effects.⁷⁸ For the sake of simplicity, here we ignore screening and consider the simple bare one-electron term in the Breit–Pauli Hamiltonian :

$$\hat{\mathbf{h}}_{SO}(\mathbf{r}) = \frac{\alpha_0^2}{2} \sum_{i=1}^{N_{elec}} \sum_{N=1}^{N_{nuc}} \frac{Z_N}{|\hat{\mathbf{r}}_i - \hat{\mathbf{R}}_N|^3} \left((\hat{\mathbf{r}}_i - \hat{\mathbf{R}}_N) \times \hat{\mathbf{p}}_i \right) \cdot \hat{\mathbf{s}}_i \quad (21)$$

where α_0 is the fine structure constant. Indexes i and N label electrons and nuclei, respectively, with $\hat{\mathbf{r}}_i$ and $\hat{\mathbf{R}}_N$ being their corresponding position operators. $\hat{\mathbf{p}}_i$ and $\hat{\mathbf{s}}_i$ are linear momentum and spin operators, respectively, for electron i . Z_N is the charge of nucleus N .

The matrix representation of the spin–orbit Hamiltonian term in the atomic orbital basis contains elements proportional to the scalar product between electronic orbital angular momentum (\mathbf{L}_{elec}) and spin (\mathbf{S}) angular momentum. This leads to a block structure as in Eq. 16, with off-diagonal blocks introducing complex-valued terms into the electronic Hamiltonian:

$$\mathbf{L}_{elec} \cdot \mathbf{S} \sim \begin{pmatrix} L_{\mu\nu}^z & L_{\mu\nu}^x - i L_{\mu\nu}^y \\ L_{\mu\nu}^x + i L_{\mu\nu}^y & -L_{\mu\nu}^z \end{pmatrix} \quad (22)$$

Finally we have the constraint as defined in Eq. 12 in terms of projections onto the active space,

$$\text{Tr}[\mathbf{Q}(\mathbf{P}_1 + \mathbf{P}_2)] = 0 \quad (23)$$

where $\mathbf{Q} = \mathbf{P}_L - \mathbf{P}_R$, and active space densities $\mathbf{P}_1 = \mathbf{C}\mathbf{K}_1\mathbf{C}^\dagger$ and $\mathbf{P}_2 = \mathbf{C}\mathbf{K}_2\mathbf{C}^\dagger$. Each of \mathbf{P}_L and \mathbf{P}_R has a block diagonal structure in the spinor basis with identical blocks.

2.3 Electronic Gradients for Energy and Constraints

To variationally minimize the target function subject to spin symmetry and active space projection constraints (Eq. 13), we optimize the molecular orbitals via a unitary transformation of the initial guess of coefficient matrix \mathbf{C}_0 . We define an anti-Hermitian orbital rotation matrix \mathbf{A} in the molecular orbital (MO) basis and construct the unitary transformation $\mathbf{U} = e^{\mathbf{A}}$. The orbitals are updated using this rotation matrix

$$\mathbf{C} = \mathbf{C}_0 e^{\mathbf{A}} \quad (24)$$

The gradient of the GHF energy (say, in the ground state with density matrix \mathbf{K}_g) is then (more details in Supplementary Information 6.1)

$$\nabla_{A_{pq}} E = \left(\left[(\mathbf{C}_0^\dagger \mathbf{F} \mathbf{C}_0)^\top, \mathbf{K}_g \right] \right)_{pq} \quad (25)$$

Under time-reversal symmetry, MO coefficients transform as follows:

$$\hat{T} \begin{pmatrix} c_{\mu i}^\alpha \\ c_{\mu i}^\beta \end{pmatrix} = \begin{pmatrix} -c_{\mu i}^{\beta*} \\ c_{\mu i}^{\alpha*} \end{pmatrix} \quad (26)$$

To ensure that any symmetry present in the initial guess density matrix is preserved throughout the orbital optimization, the same symmetry constraints must be imposed on the orbital

rotation matrix. To that end, note that unitarity is guaranteed for any transformation of the MO coefficients with an anti-Hermitian generator matrix \mathbf{A} . Moreover, to preserve time-reversal symmetry between the molecular orbitals, \mathbf{A} must adopt a certain structure:

$$\mathbf{A} = \begin{bmatrix} \mathbf{B} & -\mathbf{D}^* \\ \mathbf{D} & \mathbf{B}^* \end{bmatrix} \quad (27)$$

The gradient of the constraint has a similar form as the commutator in Eq. 25. Thus, the full expression for the gradient of the Lagrangian becomes

$$\nabla_{A_{pq}} \mathcal{L} = w'_1 \nabla_{A_{pq}} E_1 + w'_2 \nabla_{A_{pq}} E_2 - \lambda \nabla_{A_{pq}} \text{Tr}[\mathbf{Q}(\mathbf{P}_1 + \mathbf{P}_2)] \quad (28)$$

$$= w'_1 [\mathbf{M}_1^\top, \mathbf{K}_g] + w'_2 [\mathbf{M}_2^\top, \mathbf{K}_e] - \lambda [\mathbf{M}_Q^\top, \mathbf{K}_1 + \mathbf{K}_2] \quad (29)$$

where

$$\mathbf{M}_1 = \mathbf{C}_0^\dagger (\mathbf{F}[\mathbf{P}_g]) \mathbf{C}_0 \quad (30)$$

$$\mathbf{M}_2 = \mathbf{C}_0^\dagger (\mathbf{F}[\mathbf{P}_e]) \mathbf{C}_0 \quad (31)$$

$$\mathbf{M}_Q = \mathbf{C}_0^\dagger \mathbf{Q} \mathbf{C}_0 \quad (32)$$

When interpreting the gradient of the Lagrangian in Eq. 29, several nuances must be pointed out. First, note that each block of the rotation matrix has real and imaginary parts. Thus, the gradient in Eq. 29 must be taken w.r.t. the real and imaginary part of \mathbf{B} ($\mathbf{B}^r, \mathbf{B}^i$) and \mathbf{D} ($\mathbf{D}^r, \mathbf{D}^i$) in Eq. 27. Second, in order to maintain orthonormality of orbitals and preserve time-reversal symmetry during orbital optimization, the \mathbf{B} block should be anti-Hermitian, so that \mathbf{B}^r should be anti-symmetric and \mathbf{B}^i symmetric. Similarly, \mathbf{D} (and hence \mathbf{D}^r and \mathbf{D}^i) should be symmetric. We capture all these symmetries mathematically in Eq. 34. Third, consider the diagonal elements of the \mathbf{B} and \mathbf{D} blocks. Diagonal of \mathbf{B} corresponds to a phase change; diagonal of \mathbf{D} corresponds to mix one state with its time reversal pair,

which will be degenerate if the Hamiltonian has time-reversal symmetry. Consequently, we exclude these diagonal terms from the gradient evaluation. Fourth, note that only inter-subspace rotations within the occupied-unoccupied subspace of \mathbf{B} and \mathbf{D} blocks contribute to a change in the energy and hence only those elements in the upper triangle need to be included in the gradient calculation. Let us now be more precise mathematically. Let us divide up $\nabla_{A_{pq}} \mathcal{L} \equiv \mathbf{G}$ into four blocks as

$$\mathbf{G} = \begin{pmatrix} \mathbf{G}^{11} & \mathbf{G}^{12} \\ \mathbf{G}^{21} & \mathbf{G}^{22} \end{pmatrix} \quad (33)$$

As discussed above, imposing time-reversal structure on the rotation matrix means that we have to take gradients w.r.t. real and imaginary parts of \mathbf{B} and \mathbf{D} matrices.

$$\nabla_{\mathbf{B}^r} \mathcal{L} = (\mathbf{G}^{11} - \mathbf{G}^{11\top}) + (\mathbf{G}^{22} - \mathbf{G}^{22\top}) \quad (34a)$$

$$\nabla_{\mathbf{B}^i} \mathcal{L} = i ((\mathbf{G}^{11} + \mathbf{G}^{11\top}) - (\mathbf{G}^{22} + \mathbf{G}^{22\top})) \quad (34b)$$

$$\nabla_{\mathbf{D}^r} \mathcal{L} = (\mathbf{G}^{21} + \mathbf{G}^{21\top}) - (\mathbf{G}^{12} + \mathbf{G}^{12\top}) \quad (34c)$$

$$\nabla_{\mathbf{D}^i} \mathcal{L} = i ((\mathbf{G}^{21} + \mathbf{G}^{21\top}) + (\mathbf{G}^{12} + \mathbf{G}^{12\top})) \quad (34d)$$

Note that all four gradients above are real-valued functions. Solving a constraint optimization problem as in (Eq. 13), is usually done using SQP⁷⁹ (Sequential Quadratic Programming) algorithm which requires only the gradients of the target function (Eq. 2) and the constraint (Eq. 12). In the spirit of Ref. 61, we will initiate the orbital optimization through a two step iterative procedure: (i) a SCF step and (ii) a constrained non-self-consistent-field (nSCF) step.

2.3.1 SCF steps

In the SCF steps, the complex MO coefficients are updated by solving the Lagrangian in Eq. 13. A further speedup is obtained when using the direct inversion of iterative subspace

(DIIS) technique to solve the SCF problem. The gradient of Lagrangian should vanish at convergence. Thus Eq. 29, suggests that we can use the following form of error vector in DIIS:

$$\mathbf{V}_{\text{DIIS}} = w'_1[\mathbf{M}_1^T, \mathbf{K}_g] + w'_2[\mathbf{M}_2^T, \mathbf{K}_e] - \lambda[\mathbf{M}_Q^T, \mathbf{K}_1 + \mathbf{K}_2] \quad (35)$$

indicating how far the electronic densities are from the true solution. Again, in order to maintain the symmetries, the actual DIIS vector would be

$$\mathbf{V}_{\text{DIIS}} = \begin{pmatrix} \nabla_{\mathbf{B}^r} \mathcal{L} \\ \nabla_{\mathbf{B}^i} \mathcal{L} \\ \nabla_{\mathbf{D}^r} \mathcal{L} \\ \nabla_{\mathbf{D}^i} \mathcal{L} \end{pmatrix} \quad (36)$$

2.3.2 nSCF steps

For the nSCF step, we solve for new MO coefficients using fixed values of w'_1, w'_2 and $\tilde{\mathbf{F}}$. Here, $\tilde{\mathbf{F}}$ ($\tilde{\mathbf{F}}_g$ and $\tilde{\mathbf{F}}_e$ for ground and excited state, respectively) is the Fock matrix calculated for a fixed value of the density matrix. We define an auxiliary energy function of the form:

$$E_{aux} = w'_1 \text{Tr}[\tilde{\mathbf{F}}_g \mathbf{P}_g] + w'_2 \text{Tr}[\tilde{\mathbf{F}}_e \mathbf{P}_e] \quad (37)$$

Minimizing E_{aux} with the constraint on active space is equivalent to solving a Lagrangian of form

$$\mathcal{L}_{aux} = w'_1 \text{Tr}[\tilde{\mathbf{F}}_g \mathbf{P}_g] + w'_2 \text{Tr}[\tilde{\mathbf{F}}_e \mathbf{P}_e] - \lambda \text{Tr}(\mathbf{Q}(\mathbf{P}_1 + \mathbf{P}_2)) \quad (38)$$

2.4 Full SCF procedure

Finally, let us summarize the proposed procedure for calculating the energy. The idea is to solve the SCF equations to find the optimal set of orbital rotation matrices under some constraints. We work in the complex spinor basis which has a block structure as shown in Eq. 16. To enforce this block structure and maintain time reversal symmetry (TRS), we diagonalize the spin up block of the core hamiltonian and use the eigenvectors to construct orthonormal MO coefficients as Kramers restricted pairs (Eq. 26). Since the updates to this MO coefficient matrix happens through unitary rotation, the TRS relation is maintained in each SCF update (Eq. 24) until convergence.

The algorithmic steps are as follows:

1. Choose a set of MO coefficients (\mathbf{C}_{ini}); calculate \mathbf{Q} .
2. Build ground (\mathbf{P}_g) and excited (\mathbf{P}_e) state density matrices using Eq. 17
3. Build state weights (w_1 and w_2) and Fock matrices ($\mathbf{F}[\mathbf{P}_g]$ and $\mathbf{F}[\mathbf{P}_e]$) using density matrices. Calculate Fock matrices and \mathbf{Q} matrix in MO basis using Eq. 30 - 32.
4. Compute the initial DIIS error vector \mathbf{V}^0 using Eq. 35, i.e.,

$$\mathbf{V}^0 = w'_1[\mathbf{M}_0^\top[\mathbf{P}_g], \mathbf{K}_g] + w'_2[\mathbf{M}_0^\top[\mathbf{P}_e], \mathbf{K}_e] - \lambda[\mathbf{M}_Q^\top, \mathbf{K}_1 + \mathbf{K}_2] \quad (39)$$

and impose proper symmetries as in Eq. 36

5. If norm (\mathbf{V}^n) $< T_D$ (DIIS error threshold), jump to **Step 14**. Otherwise, set the initial DIIS variable \mathbf{A}^0 (Eq. 40) to $\mathbf{0}$.
6. Solve the nSCF problem for the new \mathbf{C} and λ using SQP. The nSCF threshold for the norm of the gradient and the constraint is set to norm (\mathbf{V}^0)/100.
7. (DIIS iteration starts) Build density matrices from new \mathbf{C} using Eq. 17

8. Build state weights and calculate Fock and \mathbf{Q} matrices in MO basis
9. Calculate the DIIS error vector \mathbf{V}^n at iteration n .
10. Solve the nSCF problem for new \mathbf{C} and λ using SQP. The nSCF threshold for the norm of the gradient and the constraint is set to norm $(\mathbf{V}^n)/100$.
11. Calculate the DIIS variable at iteration n :

$$\mathbf{A}^n = \log \left(\mathbf{C}_{\text{ini}}^\dagger \mathbf{C} \right) \quad (40)$$

12. If norm $(\mathbf{V}^n) < T_D$, exit the iteration and jump to **Step 14**. Otherwise, use DIIS algorithm to calculate new \mathbf{C} . and set \mathbf{C} to be $\mathbf{C}_{\text{ini}} e^{\Delta \mathbf{A}}$.
13. Return to **Step 7**
14. DIIS convergence achieved.

3 Numerical Results

We have implemented the algorithm described above in a development version of Q-Chem⁸⁰ and applied it to a charge transfer system. The phenoxy-phenol (ph-ph) system has been studied before within a restricted open-shell framework using hDSC.^{46,61} The result is presented in Fig. 4, where the reaction coordinate is the displacement of bridging hydrogen between oxygen atoms on symmetrically located fragments. Note that each curve is doubly degenerate, representing the symmetry between time-reversal configuration pairs in the ground and excited states. As established previously, we find a very natural curve crossing here as the hydrogen position is correlated with the position of the electron, i.e., this model represents a Proton-Coupled Electron Transfer (PCET)⁸¹ process.

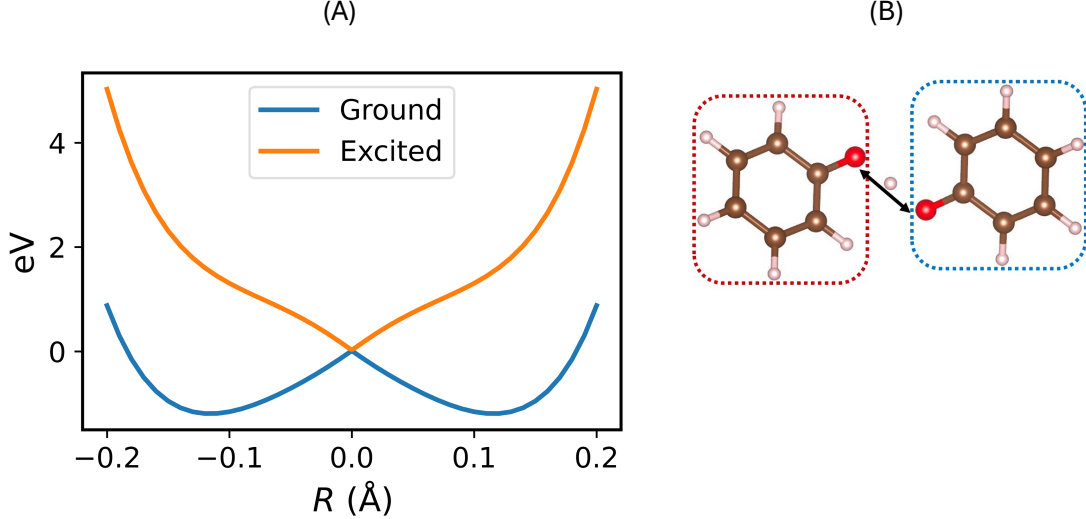


Figure 4: Potential energy curves for a bridging hydrogen transferring between two symmetrically located fragments. (A) Ground and excited energy surfaces shown in blue and orange, respectively. (B) Molecular geometry of the phenoxy–phenol (ph–ph) system, illustrating the hydrogen transfer pathway (black arrow) between the two ring fragments highlighted in red and blue. The reaction coordinate R represents the displacement of the transferring hydrogen relative to the midpoint between the two oxygen atoms. The internuclear distance between oxygen atoms is 2.459 Å. See Supplementary Information for Cartesian coordinates of molecular geometry.

3.1 Scaling spin-orbit coupling strength

Fig. 4 mimics the results in Ref.⁴⁶ To learn fundamentally new physics, we next investigate the effect of increasing spin-orbit coupling on potential energy surfaces and crossings. We plot the energy surfaces for a range of spin-orbit coupling strengths in Fig. 5. The scaling parameter η is a prefactor in Eq. 21.

Two features emerge from these figures. First, the general shape of the curve can change with η , but the algorithm appears robust and our curves remain smooth. Second and most importantly, we correctly find that the energy gap in the central crossing region (i.e. the diabatic coupling) increases with η . Panel B zooms in the avoided crossing region of the PES for these scaling parameters. This feature reminds us how important SOC can and will be for investigating electron and hole transfer for systems with heavy metals. Panel C highlights the fact that the energy gap scales quadratically, as one should expect.

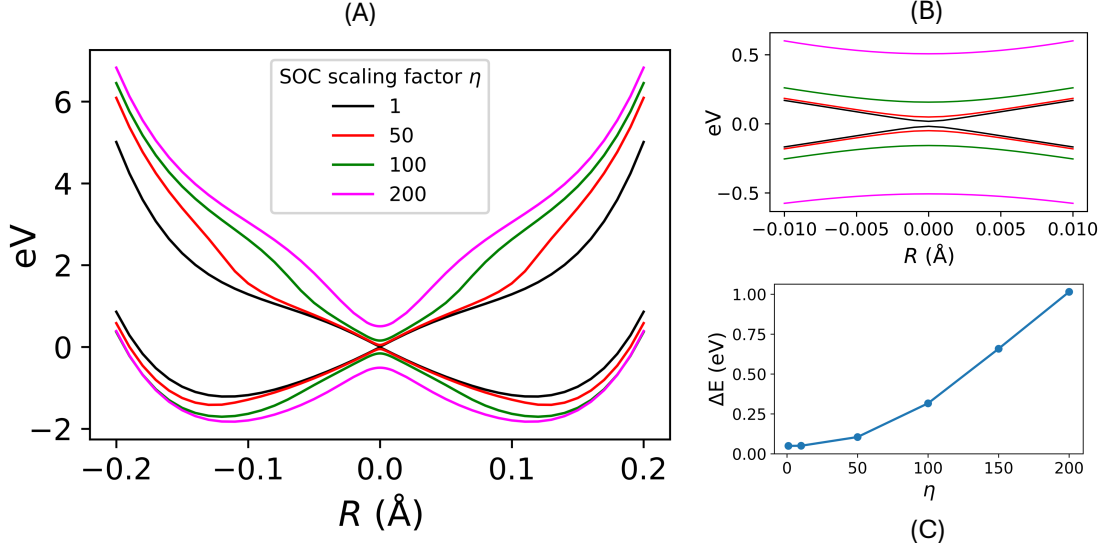


Figure 5: Effect of increasing spin-orbit coupling strength. (A) Ground and excited state PES. The energies are shifted to set zero as mean of two surfaces in the middle. The SOC term in Eq. 21 is scaled by a factor η for all geometries along the reaction coordinate. Each color represents the two PES for $\eta = [1, 50, 100, 200]$. (B) PES near avoided crossing region. (C) Energy gap between ground and excited state at $R = 0.0$ Å for different values of η .

3.2 Electron density in active orbitals

Starting from the usual occupied-orbital expansion, the total (spin-summed) real-space electron density is defined as

$$\rho(\mathbf{r}) = \sum_{i \in \text{occ}} \int \chi_i^\dagger(\mathbf{r}, \omega) \chi_i(\mathbf{r}, \omega) d\omega, \quad (41)$$

where the integration is carried out over the spin coordinate ω . Using expansion in terms of spin orbitals from Eq. 14 and orthonormality relation $\langle \alpha | \beta \rangle = 0$,

$$\rho(\mathbf{r}) = \sum_{i \in \text{occ}} \left(|\psi_i^\alpha(\mathbf{r})|^2 + |\psi_i^\beta(\mathbf{r})|^2 \right) \quad (42)$$

Substituting the orbital expansion from Eq. 15 the electron density can be written in terms of diagonal blocks of density matrix and the real-space atomic orbitals

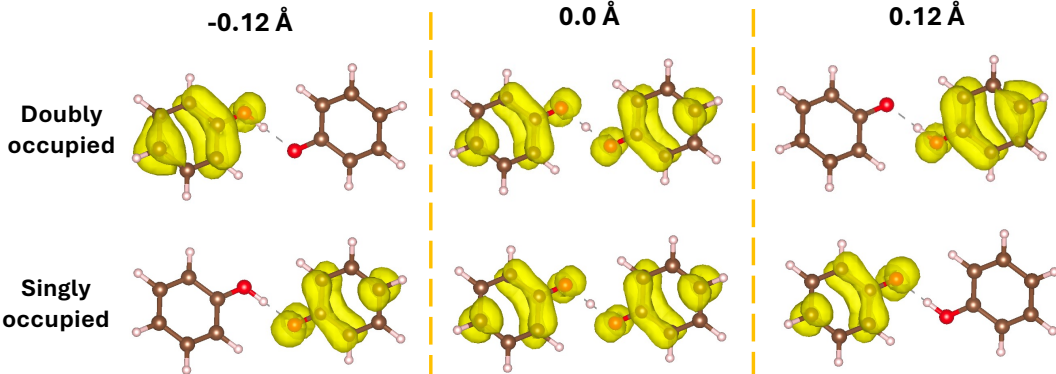
$$\rho(\mathbf{r}) = \sum_{\mu\nu} (\mathbf{P}_{\mu\nu}^{\alpha\alpha} + \mathbf{P}_{\mu\nu}^{\beta\beta}) \phi_{\mu}(\mathbf{r}) \phi_{\nu}(\mathbf{r}) \quad (43)$$

Because \mathbf{P} is Hermitian ($\mathbf{P}^T = \mathbf{P}^*$), $\rho(\mathbf{r})$ depends only on the real part of these elements. Electron density plots (along the charge transfer reaction coordinate) for the two active orbitals (i.e., $\mathbf{P}_j = \mathbf{C}\mathbf{K}_j\mathbf{C}^{\dagger}$ where $j \in \{1, 2\}$) are drawn in Fig. 6A. These drawing represent the singly and doubly occupied orbitals and are shown for three geometries along the reaction coordinate: the left well minima (-0.12 Å), the midpoint (0.0 Å) and the right well (0.12 Å). A comparative plot is shown in Figure. 6B for the strong SOC case ($\eta = 200$).

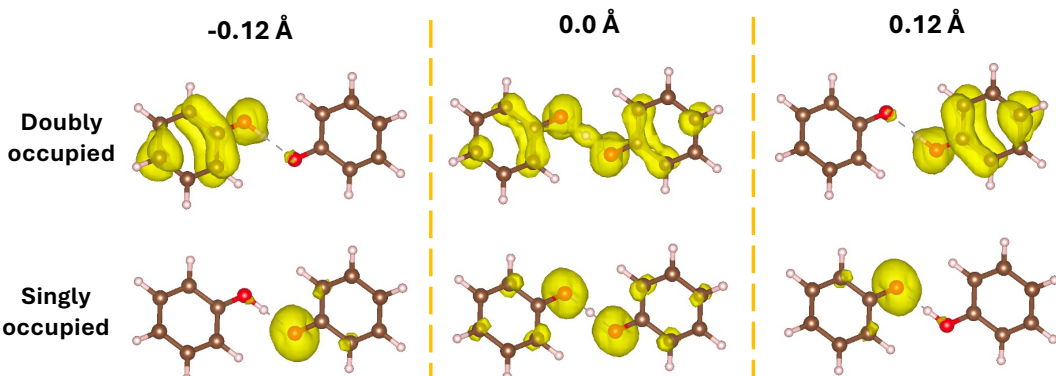
4 Outlook and Conclusions

We have presented a method to calculate CT states for molecular systems with an odd number of electrons, keeping track of each state's spin properties. The end result is a fast and efficient CASSCF(1,2)/CASSCF(3,2) framework for studying charge transfer in the presence of SOC. To that end, we have investigated a range of SOC strength values and show that energy gap between ground and excited states scales quadratically. While our work here has focused on second row elements (with weak spin-orbit coupling), our approach should be even more important for third row elements, with more SOC and thus a larger entanglement of spin with electron transfer.

Looking forward, one can envision three important future directions. First, one must wonder: for a four state (2×2) curve crossing, what are the most natural diabatic states that can be constructed so as to preserve the orbital and spin character of a given electronic states. To that end, in a forthcoming article, we will explore different means of constructing diabatic states through adiabatic-to-diabatic transformations where spin cannot be ignored. Second, as we emphasized in the introduction, one would like a means to run dynamics that



(A) Active orbital electron density with SOC strength $\eta = 1$.



(B) Active orbital electron density with SOC strength $\eta = 200$.

Figure 6: A comparison of the active orbital electron densities for two different SOC coupling strengths at $R = [-0.12 \text{ \AA}, 0.0 \text{ \AA}, 0.12 \text{ \AA}]$

conserve both the total energy and the total momentum. Now, whereas BO dynamics along a surface $E_{\text{BO}}(\mathbf{R})$ (for the most part) ignore electronic momentum, our research group has shown over the past several years⁸² that dynamics along a phase space electronic structure surface ($E_{\text{PS}}(\mathbf{R}, \mathbf{P})$ parameterized by both nuclear position and momentum) does conserve electronic momentum. Thus, in the immediate future, it will be quite illuminating to extend the current eDSC/hDSC approach to diagonalize $H_{\text{PS}}(\mathbf{R}, \mathbf{P})$ rather than $H_{\text{BO}}(\mathbf{R})$. Note that, for the former (as opposed to the latter), the degeneracy of Kramers doublets is lifted because nuclear motion breaks the time reversibility of the electronic Hamiltonian, and so our present algorithm will need to be modified. Third and finally, one would like to explore the extension of the current algorithm to include magnetic fields,^{83–85} another perturbation that breaks

time-reversibility and leads to highly interesting momentum effects. The bottom line is that, once we begin to explore curve crossing and electron transfer in the presence of spin degrees of freedom, there is still a great deal of unexplored terrain for theoretical chemistry; the present algorithm is clearly just the tip of the iceberg.

5 Acknowledgments

This work has been supported by the U.S. Department of Energy, Office of Science, Office of Basic Energy Sciences, under Award no. DE-SC0025393. We have also used resources of the National Energy Research Scientific Computing Center (NERSC), a U.S. Department of Energy Office of Science User Facility operated under Contract no. DE-AC02-05CH11231.

6 Supplementary Information

6.1 Energy gradients w.r.t complex-valued orbital rotation

Here, we highlight the energy gradient expression w.r.t the orbital rotation matrix \mathbf{A} . Let us introduce the anti-Hermitian operator

$$\hat{\mathbf{A}} = \sum_{pq} A_{pq} a_p^\dagger a_q, \quad \hat{\mathbf{A}}^\dagger = -\hat{\mathbf{A}}^\dagger \quad (44)$$

$$A_{pq} = A_{pq}^r + i A_{pq}^i \quad (45)$$

with $a_p^\dagger (a_q)$ being the creation (annihilation) operator for spin orbital $\chi_p (\chi_q)$. The complex-valued parameters A_{pq} are expressed in terms of its real and imaginary parts. Note that both A_{pq}^r and A_{pq}^i are real parameters and anti-Hermiticity is ensured by requiring them to

be anti-symmetric and symmetric, respectively

$$A_{pq}^r = -A_{qp}^r \quad (46a)$$

$$A_{pq}^i = A_{qp}^i \quad (46b)$$

Following ref.,⁸⁶ the operator $\hat{\mathbf{A}}$ can now be expressed as

$$\hat{\mathbf{A}} = \sum_{p>q} A_{pq}^r (a_p^\dagger a_q - a_q^\dagger a_p) + i \left(\sum_p A_{pp}^i a_p^\dagger a_p + \sum_{p>q} A_{pq}^i (a_p^\dagger a_q + a_q^\dagger a_p) \right) \quad (47)$$

$$= \sum_{p>q} A_{pq}^r E_{pq}^- + i \left(\sum_p A_{pp}^i N_p + \sum_{p>q} A_{pq}^i E_{pq}^+ \right) \quad (48)$$

$$\left. \frac{\partial E}{\partial A_{pq}^r} \right|_{\mathbf{A}=0} = \langle [E_{pq}^-, H] \rangle = ([\mathbf{F}, \mathbf{P}]_{qp} - [\mathbf{F}, \mathbf{P}]_{pq}), \quad (p > q) \quad (49)$$

$$\left. \frac{\partial E}{\partial A_{pq}^i} \right|_{\mathbf{A}=0} = i \langle [E_{pq}^+, H] \rangle = i ([\mathbf{F}, \mathbf{P}]_{qp} + [\mathbf{F}, \mathbf{P}]_{pq}), \quad (p > q) \quad (50)$$

The result for the upper triangle follows directly from the symmetry relations in Eq. 46.

$$\frac{\partial E}{\partial A_{qp}^r} = -\frac{\partial E}{\partial A_{pq}^r}, \quad \frac{\partial E}{\partial A_{qp}^i} = -\frac{\partial E}{\partial A_{pq}^i}. \quad (51)$$

The commutator can be simplified in the MO basis which diagonalizes the density matrix. If \mathbf{C} represents the MO coefficients in the orthonormal AO basis, then $\mathbf{C}^\dagger \mathbf{C} = \mathbf{C} \mathbf{C}^\dagger = \mathbf{I}$. The matrix transformations between the orthonormal AO basis and the MO basis are as follows:

$$\mathbf{K} = \mathbf{C}^\dagger \mathbf{P} \mathbf{C} \quad (52)$$

$$\mathbf{F}^{MO} = \mathbf{C}^\dagger \mathbf{F} \mathbf{C} \quad (53)$$

In the MO basis, the commutator becomes

$$\mathbf{C}^\dagger([\mathbf{F}, \mathbf{P}])\mathbf{C} = [\mathbf{F}^{MO}, \mathbf{K}] \quad (54)$$

where $\mathbf{K} = \text{diag}(n_1, n_2, \dots)$ is a diagonal matrix with $n_j \in \{0, 1\}$.

$$([\mathbf{F}^{MO}, \mathbf{K}])_{pq} = (n_q - n_p)\mathbf{F}_{pq}^{MO} \quad (55)$$

6.2 Geometry of phenoxy-phenol (ph-ph) system

C -3.339987 1.236679 -0.292676
 C -2.215700 0.395873 -0.461119
 C -2.260068 -0.923462 0.044893
 C -3.395583 -1.374735 0.696165
 C -4.500797 -0.539367 0.860105
 C -4.462623 0.765553 0.361575
 O -1.170747 0.860673 -1.076240
 H -1.404926 -1.560653 -0.084864
 H -3.424139 -2.378976 1.078261
 H -5.377346 -0.897488 1.367665
 H -5.313306 1.410015 0.488105
 H -3.290462 2.235719 -0.683604
 C 2.967610 -0.964278 -0.250086
 C 1.842996 -0.128779 -0.443279
 C 1.884680 1.202903 0.030149
 C 3.017817 1.671520 0.673563
 C 4.123167 0.841308 0.861788
 C 4.087496 -0.476001 0.395845

O 0.800605 -0.609058 -1.049392
H 1.029641 1.836307 -0.118287
H 3.044634 2.685260 1.030351
H 4.998118 1.212844 1.362705
H 4.938888 -1.115655 0.540969
H 2.920157 -1.972439 -0.616477
H -0.579299 0.419269 -1.076240

References

- (1) Meech, S.; Hoff, A.; Wiersma, D. Role of charge-transfer states in bacterial photosynthesis. *Proceedings of the National Academy of Sciences* **1986**, *83*, 9464–9468.
- (2) Wasielewski, M. R. Photoinduced electron transfer in supramolecular systems for artificial photosynthesis. *Chemical reviews* **1992**, *92*, 435–461.
- (3) Møller, I. M. Plant mitochondria and oxidative stress: electron transport, NADPH turnover, and metabolism of reactive oxygen species. *Annual review of plant biology* **2001**, *52*, 561–591.
- (4) Massey, V. Activation of molecular oxygen by flavins and flavoproteins. *Journal of Biological Chemistry* **1994**, *269*, 22459–22462.
- (5) Siedow, J. N.; Umbach, A. L. Plant mitochondrial electron transfer and molecular biology. *The Plant Cell* **1995**, *7*, 821.
- (6) Forrest, S. R.; Thompson, M. E. Introduction: organic electronics and optoelectronics. *Chemical Reviews* **2007**, *107*, 923–925.

(7) Deibel, C.; Dyakonov, V. Polymer–fullerene bulk heterojunction solar cells. *Reports on Progress in Physics* **2010**, *73*, 096401.

(8) Coropceanu, V.; Cornil, J.; da Silva Filho, D. A.; Olivier, Y.; Silbey, R.; Brédas, J.-L. Charge transport in organic semiconductors. *Chemical reviews* **2007**, *107*, 926–952.

(9) Zhu, X.-Y.; Yang, Q.; Muntwiler, M. Charge-transfer excitons at organic semiconductor surfaces and interfaces. *Accounts of chemical research* **2009**, *42*, 1779–1787.

(10) Ostroverkhova, O. Organic optoelectronic materials: mechanisms and applications. *Chemical reviews* **2016**, *116*, 13279–13412.

(11) Etherington, M. K.; Gibson, J.; Higginbotham, H. F.; Penfold, T. J.; Monkman, A. P. Revealing the spin–vibronic coupling mechanism of thermally activated delayed fluorescence. *Nature Communications* **2016**, *7*, 13680.

(12) Wong, M. Y.; Zysman-Colman, E. Purely organic thermally activated delayed fluorescence materials for organic light-emitting diodes. *Advanced Materials* **2017**, *29*, 1605444.

(13) Zhang, T.; Xiao, Y.; Wang, H.; Kong, S.; Huang, R.; Ka-Man Au, V.; Yu, T.; Huang, W. Highly twisted thermally activated delayed fluorescence (TADF) molecules and their applications in organic light-emitting diodes (OLEDs). *Angewandte Chemie International Edition* **2023**, *62*, e202301896.

(14) Marcus, R. A. On the theory of oxidation-reduction reactions involving electron transfer. I. *The Journal of chemical physics* **1956**, *24*, 966–978.

(15) Hush, N. S. Adiabatic theory of outer sphere electron-transfer reactions in solution. *Transactions of the Faraday Society* **1961**, *57*, 557.

(16) Levich, V. G.; Dogonadze, R. R. Adiabatic theory of electron-processes in solution. *Collection of Czechoslovak Chemical Communications* **1961**, *26*, 193–214.

(17) Cukier, R. I.; Nocera, D. G. PROTON-COUPLED ELECTRON TRANSFER. *Annual Review of Physical Chemistry* **1998**, *49*, 337–369.

(18) Jortner, J.; Bixon, M.; Langenbacher, T.; Michel-Beyerle, M. E. Charge transfer and transport in DNA. *Proceedings of the National Academy of Sciences* **1998**, *95*, 12759–12765.

(19) Dennerl, K. Charge Transfer Reactions. *Space Science Reviews* **2010**, *157*, 57–91.

(20) Penfold, T. J.; Gindensperger, E.; Daniel, C.; Marian, C. M. Spin-vibronic mechanism for intersystem crossing. *Chemical reviews* **2018**, *118*, 6975–7025.

(21) Helmich-Paris, B. Benchmarks for electronically excited states with CASSCF methods. *Journal of Chemical Theory and Computation* **2019**, *15*, 4170–4179.

(22) Athavale, V.; Teh, H.-H.; Subotnik, J. E. On the inclusion of one double within CIS and TDDFT. *The Journal of Chemical Physics* **2021**, *155*.

(23) Subotnik, J. E.; Jain, A.; Landry, B.; Petit, A.; Ouyang, W.; Bellonzi, N. Understanding the surface hopping view of electronic transitions and decoherence. *Annual review of physical chemistry* **2016**, *67*, 387–417.

(24) Crespo-Otero, R.; Barbatti, M. Recent advances and perspectives on nonadiabatic mixed quantum–classical dynamics. *Chemical reviews* **2018**, *118*, 7026–7068.

(25) Tapavicza, E.; Tavernelli, I.; Rothlisberger, U. Trajectory Surface Hopping within Linear Response Time-Dependent<? format?> Density-Functional Theory. *Physical review letters* **2007**, *98*, 023001.

(26) Mai, S.; Marquetand, P.; González, L. Nonadiabatic dynamics: The SHARC approach. *Wiley Interdisciplinary Reviews: Computational Molecular Science* **2018**, *8*, e1370.

(27) González, L.; Escudero, D.; Serrano-Andrés, L. Progress and challenges in the calculation of electronic excited states. *ChemPhysChem* **2012**, *13*, 28–51.

(28) Lischka, H.; Nachtigallova, D.; Aquino, A. J.; Szalay, P. G.; Plasser, F.; Machado, F. B.; Barbatti, M. Multireference approaches for excited states of molecules. *Chemical reviews* **2018**, *118*, 7293–7361.

(29) Matsika, S. Electronic structure methods for the description of nonadiabatic effects and conical intersections. *Chemical Reviews* **2021**, *121*, 9407–9449.

(30) Dergachev, I. D.; Dergachev, V. D.; Rooein, M.; Mirzanejad, A.; Varganov, S. A. Predicting kinetics and dynamics of spin-dependent processes. *Accounts of Chemical Research* **2023**, *56*, 856–866.

(31) Nelson, T.; Fernandez-Alberti, S.; Roitberg, A. E.; Tretiak, S. Nonadiabatic Excited-State Molecular Dynamics: Modeling Photophysics in Organic Conjugated Materials. *Accounts of Chemical Research* **2014**, *47*, 1155–1164.

(32) Prezhdo, O. V. Modeling non-adiabatic dynamics in nanoscale and condensed matter systems. *Accounts of Chemical Research* **2021**, *54*, 4239–4249.

(33) Mei, Y.; Yang, W. Charge transfer excitation energies from ground state density functional theory calculations. *The Journal of Chemical Physics* **2019**, *150*.

(34) Fischer, S. A.; Habenicht, B. F.; Madrid, A. B.; Duncan, W. R.; Prezhdo, O. V. Regarding the validity of the time-dependent Kohn–Sham approach for electron-nuclear dynamics via trajectory surface hopping. *The Journal of Chemical Physics* **2011**, *134*.

(35) Herbert, J. M.; Mandal, A. *Time-dependent density functional theory*; Jenny Stanford Publishing, 2022; pp 361–404.

(36) Bernard, Y. A.; Shao, Y.; Krylov, A. I. General formulation of spin-flip time-dependent density functional theory using non-collinear kernels: Theory, implementation, and benchmarks. *The Journal of chemical physics* **2012**, *136*.

(37) Shao, Y.; Head-Gordon, M.; Krylov, A. I. The spin–flip approach within time-dependent density functional theory: Theory and applications to diradicals. *The Journal of Chemical Physics* **2003**, *118*, 4807–4818.

(38) Levine, B. G.; Ko, C.; Quenneville, J.; Martinez, T. J. Conical Intersections and Double Excitations in Time-Dependent Density Functional Theory. *Molecular Physics* **2006**, *104*, 1039–1051.

(39) Taylor, J. T.; Tozer, D. J.; Curchod, B. F. On the description of conical intersections between excited electronic states with LR-TDDFT and ADC (2). *The Journal of chemical physics* **2023**, *159*.

(40) Wu, Q.; Cheng, C.-L.; Van Voorhis, T. Configuration interaction based on constrained density functional theory: A multireference method. *The Journal of Chemical Physics* **2007**, *127*.

(41) Wu, Q.; Van Voorhis, T. Constrained Density Functional Theory and Its Application in Long-Range Electron Transfer. *Journal of Chemical Theory and Computation* **2006**, *2*, 765–774.

(42) Wu, Q.; Voorhis, T. V. Extracting electron transfer coupling elements from constrained density functional theory. *Journal of Chemical Physics* **2006**, *125*, 164105.

(43) Mavros, M. G.; Voorhis, T. V. Communication: CDFT-CI couplings can be unreliable when there is fractional charge transfer. *Journal of Chemical Physics* **2015**, *143*, 231102.

(44) Roos, B. O.; Taylor, P. R.; Siegbahn, P. E. A complete active space SCF method (CASSCF) using a density matrix formulated super-CI approach. *Chemical Physics* **1980**, *48*, 157–173.

(45) Siegbahn, P. E.; Almlöf, J.; Heiberg, A.; Roos, B. O. The complete active space SCF

(CASSCF) method in a Newton–Raphson formulation with application to the HNO molecule. *The Journal of Chemical Physics* **1981**, *74*, 2384–2396.

(46) Qiu, T.; Bian, X.; Tao, Z.; Subotnik, J. E. A fast and smooth one-electron approach for investigating charge transfer states and D1–D0 crossings for systems with odd numbers of electrons. *The Journal of Chemical Physics* **2024**, *160*.

(47) Fedorov, D. G.; Koseki, S.; Schmidt, M. W.; Gordon, M. S. Spin-orbit coupling in molecules: Chemistry beyond the adiabatic approximation. *International Reviews in Physical Chemistry* **2003**, *22*, 551–592.

(48) Aquilante, F.; Autschbach, J.; Baiardi, A.; Battaglia, S.; Borin, V. A.; Chibotaru, L. F.; Conti, I.; De Vico, L.; Delcey, M.; Ferré, N.; others Modern quantum chemistry with [Open] Molcas. *The Journal of chemical physics* **2020**, *152*.

(49) Plasser, F.; Lischka, H.; Shepard, R.; Szalay, P. G.; Pitzer, R. M.; Alves, R. L.; Aquino, A. J.; Autschbach, J.; Barbatti, M.; Carvalho, J. R.; others COLUMBUS-An Efficient and General Program Package for Ground and Excited State Computations Including Spin–Orbit Couplings and Dynamics. *The Journal of Physical Chemistry A* **2025**, *129*, 6482–6517.

(50) Neese, F.; Wennmohs, F.; Becker, U.; Ripplinger, C. The ORCA quantum chemistry program package. *The Journal of chemical physics* **2020**, *152*.

(51) Zaari, R. R.; Varganov, S. A. Nonadiabatic transition state theory and trajectory surface hopping dynamics: intersystem crossing between 3B1 and 1A1 states of SiH2. *The Journal of Physical Chemistry A* **2015**, *119*, 1332–1338.

(52) Fedorov, D. A.; Pruitt, S. R.; Keipert, K.; Gordon, M. S.; Varganov, S. A. Ab initio multiple spawning method for intersystem crossing dynamics: Spin-forbidden transitions between 3B1 and 1A1 states of GeH2. *The Journal of Physical Chemistry A* **2016**, *120*, 2911–2919.

(53) Fedorov, D. A.; Lykhin, A. O.; Varganov, S. A. Predicting intersystem crossing rates with AIMS-DFT molecular dynamics. *The Journal of Physical Chemistry A* **2018**, *122*, 3480–3488.

(54) Jenkins, A. J.; Liu, H.; Kasper, J. M.; Frisch, M. J.; Li, X. Variational relativistic two-component complete-active-space self-consistent field method. *Journal of Chemical Theory and Computation* **2019**, *15*, 2974–2982.

(55) Kasper, J. M.; Jenkins, A. J.; Sun, S.; Li, X. Perspective on Kramers symmetry breaking and restoration in relativistic electronic structure methods for open-shell systems. *The Journal of Chemical Physics* **2020**, *153*.

(56) Liao, C.; Hoyer, C. E.; Banerjee Ghosh, R.; Jenkins, A. J.; Knecht, S.; Frisch, M. J.; Li, X. Comparison of Variational and Perturbative Spin–Orbit Coupling within Two-Component CASSCF. *The Journal of Physical Chemistry A* **2024**, *128*, 2498–2506.

(57) Ganyushin, D.; Neese, F. A fully variational spin-orbit coupled complete active space self-consistent field approach: Application to electron paramagnetic resonance g-tensors. *The Journal of Chemical Physics* **2013**, *138*.

(58) Marian, C. M. Understanding and controlling intersystem crossing in molecules. *Annual review of physical chemistry* **2021**, *72*, 617–640.

(59) Kramers, H. A. Théorie générale de la rotation paramagnétique dans les cristaux. *Proc. Acad. Amst* **1930**, *33*.

(60) Wigner, E. P. *Über die Operation der Zeitumkehr in der Quantenmechanik*; Springer, 1993.

(61) Qiu, T.; Subotnik, J. E. An Efficient Algorithm for Constrained CASSCF (1, 2) and CASSCF (3, 2) Simulations as Relevant to Electron and Hole Transfer Problems. *Journal of Chemical Theory and Computation* **2024**, *20*, 8960–8969.

(62) Nitzan, A. *Chemical Dynamics in Condensed Phases*; Oxford University Press: USA, 2006.

(63) Bloom, B. P.; Paltiel, Y.; Naaman, R.; Waldeck, D. H. Chiral induced spin selectivity. *Chemical Reviews* **2024**, *124*, 1950–1991.

(64) Bian, X.; Tao, Z.; Wu, Y.; Rawlinson, J.; Littlejohn, R. G.; Subotnik, J. E. Total angular momentum conservation in ab initio Born-Oppenheimer molecular dynamics. *Physical Review B* **2023**, *108*, L220304.

(65) Tao, Z.; Qiu, T.; Bhati, M.; Bian, X.; Duston, T.; Rawlinson, J.; Littlejohn, R. G.; Subotnik, J. E. Practical phase-space electronic Hamiltonians for ab initio dynamics. *The Journal of Chemical Physics* **2024**, *160*.

(66) Naaman, R.; Waldeck, D. H. What Can CISS Teach Us about Electron Transfer? *The Journal of Physical Chemistry Letters* **2024**, *15*, 11002–11006.

(67) Abedi, A.; Maitra, N. T.; Gross, E. K. U. Exact Factorization of the Time-Dependent Electron-Nuclear Wave Function. *Physical Review Letters* **2010**, *105*, 123002.

(68) Abedi, A.; Maitra, N. T.; Gross, E. K. U. Correlated electron-nuclear dynamics: Exact factorization of the molecular wavefunction. *Journal of Chemical Physics* **2012**, *137*, 22A530.

(69) Stuber, J. L.; Paldus, J. Symmetry breaking in the independent particle model. *Fundamental world of quantum chemistry* **2003**, 67–139.

(70) Jiménez-Hoyos, C. A.; Henderson, T. M.; Scuseria, G. E. Generalized hartree–fock description of molecular dissociation. *Journal of chemical theory and computation* **2011**, *7*, 2667–2674.

(71) Hammes-Schiffer, S.; Andersen, H. C. The advantages of the general Hartree–Fock

method for future computer simulation of materials. *The Journal of chemical physics* **1993**, *99*, 1901–1913.

(72) Fedorov, D. G.; Gordon, M. S. A study of the relative importance of one and two-electron contributions to spin–orbit coupling. *The Journal of Chemical Physics* **2000**, *112*, 5611–5623.

(73) Boettger, J. C. Approximate two-electron spin-orbit coupling term for density-functional-theory DFT calculations using the Douglas-Kroll-Hess transformation. *Physical Review B* **2000**, *62*, 7809.

(74) Heß, B. A.; Marian, C. M.; Wahlgren, U.; Gropen, O. A mean-field spin-orbit method applicable to correlated wavefunctions. *Chemical Physics Letters* **1996**, *251*, 365–371.

(75) Tatchen, J.; Marian, C. M. On the performance of approximate spin–orbit Hamiltonians in light conjugated molecules: the fine-structure splitting of HC6H+, NC5H+, and NC4N+. *Chemical physics letters* **1999**, *313*, 351–357.

(76) Liu, J.; Cheng, L. An atomic mean-field spin-orbit approach within exact two-component theory for a non-perturbative treatment of spin-orbit coupling. *The Journal of Chemical Physics* **2018**, *148*.

(77) Koseki, S.; Gordon, M. S.; Schmidt, M. W.; Matsunaga, N. Main group effective nuclear charges for spin-orbit calculations. *The Journal of Physical Chemistry* **1995**, *99*, 12764–12772.

(78) Ehrman, J.; Martinez-Baez, E.; Jenkins, A. J.; Li, X. Improving one-electron exact-two-component relativistic methods with the Dirac–Coulomb–Breit-parameterized effective spin–orbit coupling. *Journal of Chemical Theory and Computation* **2023**, *19*, 5785–5790.

(79) Nocedal, J.; Wright, S. J. *Numerical Optimization*; Springer New York, 2006.

(80) Epifanovsky, E.; Gilbert, A. T.; Feng, X.; Lee, J.; Mao, Y.; Mardirossian, N.; Pokhilko, P.; White, A. F.; Coons, M. P.; Dempwolff, A. L.; others Software for the frontiers of quantum chemistry: An overview of developments in the Q-Chem 5 package. *The Journal of chemical physics* **2021**, *155*, 084801.

(81) Hammes-Schiffer, S. Proton-coupled electron transfer: Moving together and charging forward. *Journal of the American Chemical Society* **2015**, *137*, 8860–8871.

(82) Tao, Z.; Qiu, T.; Bian, X.; Duston, T.; Bradbury, N.; Subotnik, J. E. A basis-free phase space electronic Hamiltonian that recovers beyond Born–Oppenheimer electronic momentum and current density. *The Journal of Chemical Physics* **2025**, *162*.

(83) Bhati, M.; Tao, Z.; Bian, X.; Rawlinson, J.; Littlejohn, R.; Subotnik, J. E. A Phase-Space Electronic Hamiltonian for Molecules in a Static Magnetic Field. I: Conservation of Total Pseudomomentum and Angular Momentum. *The Journal of Physical Chemistry A* **2025**, *129*, 4555–4572.

(84) Bhati, M.; Tao, Z.; Bian, X.; Rawlinson, J.; Littlejohn, R.; Subotnik, J. E. A Phase-Space Electronic Hamiltonian for Molecules in a Static Magnetic Field II: Quantum Chemistry Calculations with Gauge Invariant Atomic Orbitals. *The Journal of Physical Chemistry A* **2025**, *129*, 4573–4590.

(85) Rooein, M.; Varganov, S. A. Predicting kinetics of spin-dependent reactions in an external magnetic field with nonadiabatic statistical theory. *The Journal of Chemical Physics* **2024**, *161*.

(86) Helgaker, T.; Jorgensen, P. *Molecular Electronic Structure Theory*; Wiley: New York, 2013.